Molecular isomerization induced by ultrashort infrared pulses. II. Pump-dump isomerization using pairs of time-delayed half-cycle pulses

Christoph Uiberacker* and Werner Jakubetz†

Institut für theoretische Chemie und Molekulare Strukturbiologie,

Universität Wien, Währinger Str. 17, A-1090 Wien, Austria

(Dated: March 16, 2004)

Abstract

We investigate population transfer across the barrier in a double-well potential, induced by a pair of time-delayed single-lobe half-cycle pulses. We apply this setup both to a one- dimensional (1d) quartic model potential and to a three-dimensional potential representing HCN→HNC isomerization. Overall the results for the two systems are similar, although in the 3d system some additional features appear not seen in the 1d case. The generic mechanism of population transfer is the preparation by the pump pulse of a wavepacket involving delocalized states above the barrier, followed by the essentially 1d motion of the delocalized part of wavepacket across the barrier, and the eventual de-excitation by the dump pulse to localized states in the other well. The correct timing is given by the well-to-well passage time of the wavepacket and its recurrence properties, and by the signs of the field lobes which determine the direction and acceleration or deceleration of the wavepacket motion. In the 3d system an additional pump-pump-dump mechanism linked to wavepacket motion in the reagent well can mediate isomerization. Since the transfer time and the pulse durations are of the same order of magnitude, there is also a marked dependence of the dynamics and the transfer yield on the pulse duration. Our analysis also sheds light on the pronounced carrier envelope phase dependence previously observed for isomerization and molecular dissociation with one-cycle and sub-one-cycle pulses.

*Electronic address: christoph.uiberacker@univie.ac.at

†Electronic address: werner.jakubetz@univie.ac.at

I. INTRODUCTION

In a part I of this series [1] we investigated population transfer in a three- dimensional (3d) double-well potential using single few-cycle and sub-one cycle laser pulses, taking the HCN→HNC isomerization [2–5] as model system. We found that isomerization can be driven by an effective one-cycle pulse. However, only the pattern of a positive lobe followed by a negative one leads to successful isomerization, which means there is an extremely pronounced dependence of the transfer probability on the carrier envelope phase (CEP).[6] The transfer across the barrier proceeds by an internal pump-dump mechanism, where the pump is triggered by the first lobe, and the dump by the second one. The timing between the two peaks, and hence the pulse duration and the effective frequency, are determined by the motion of a vibrational wavepacket across the barrier, which is prepared by the pump process and involves high-lying delocalized states. Furthermore, the analysis of the population dynamics showed that that the mechanism can be understood as an essentially one-dimensional (1d) process along the reaction coordinate, which predominantly involves bend motion. [2, 3]

These findings set the stage for the present paper. We replace the internal pump-dump mechanism by a pump-dump setup [7, 8] using pairs single-lobe half- cycle pulses [9] with variable time-delay. In order to map out the generic properties of the process, and also to facilitate the analysis and visualization of the underlying wavepacket dynamics, in parallel to the 3d simulations we also use a 1d double- well model constructed as a piecewise quartic potential. This choice makes the model to resemble the realistic molecular system, which possesses a strongly unsymmetric shape made up of two fairly unrelated wells. In the model system it is a straightforward task to relate the results of the pump-dump process to the formation and motion of a 1d wavepacket above and across the barrier. Its motion, and its recurrence and damping properties [10] are mapped out by varying the time delay in the pulse pair.

In addition to this standard pump-dump scenario, the signs of the two laser fields become important system parameters. Varying these signs provides additional information on the wavepacket dynamics and helps to understand the pronounced dependence of the isomerization yield on the CEP of one-cycle and sub-one-cycle pulses reported in part I. Finally, since the barrier passage time of the wavepacket and the pulse duration are of the same order of

magnitude, due to the coupling of wavepacket formation and wavepacket motion the pulse length must be expected to play a role that goes beyond the one associated with the width of the Fourier spectrum.

In our paper we present simulations addressing these points. Section II provides some technical informations: We introduce the 1d quartic model potential and compare it with the 3d HCN/HNC system, and we also describe the pulse forms we have used. Section III collects the results of the pump-dump simulations in the 1d model system and provides the analysis in terms of wavepacket formation and motion. In Section IV we report the results for the simulations on 3d HCN→HNC isomerization, and we discuss the 1d features of the dynamics as well as the deviations from simple 1d behavior. Finally, our conclusions are summarized in Section V.

II. MODEL SYSTEMS AND PULSE FORMS

In this Section we collect information on the hamiltonians used in our simulations. In particular, in Section IIA we present the 1d model system and compare it with the 3d HCN/HNC system, and in Section IIB we describe the half-cycle pulses we have used. All remaining computational details, like the propagation techniques used, are as described in part I [1]. Also as in part I, the spirit of our simulations is that of a model treatment of population transfer in double well systems by ultrashort pulses. Ignoring e.g. rotation and possible molecular ionization [11], our calculations should not be expected to accurately simulate real laboratory experiments on HCN→HNC isomerization, but to reveal the general features behind this specific process and other similar ones.

A. One- and three-dimensional double well systems

In addition to the 3-d 550 level-system, which describes the HCN→HNC isomerization, [1, 2, 5, 12], we construct a 1-dimensional piecewise quartic double-well potential of the form

$$V(x) = \begin{cases} \dfrac{(x/\alpha_l)^4}{64D_l} - \dfrac{(x/\alpha_l)^2}{4} & , \quad x < 0 \\ \dfrac{(x/\alpha_r)^4}{64D_r} - \dfrac{(x/\alpha_r)^2}{4} & , \quad x \geq 0 \end{cases} \tag{1}$$

where the distance x is the transfer coordinate for population transfer from well to well, D_l and D_r are the well depths of the left and right wells, respectively, and α_l and α_r are distance scaling factors used to adjust the potential.

Our piecewise definition provides flexibility in adjusting the asymmetry of the potential and takes care of the fact that in a system like HCN/HNC the potential minima correspond to two independent entities, with a coupling mechanism producing a double well form. Tuning the four potential parameters in Eq. 1, the reduced mass, and a dipole function μ assumed to be constant, the states in the well and the dipole matrix elements can be adjusted to resemble those of the bend states of the 3d hamiltonian used in the simulations of HCH→HNC isomerization. Corresponding parameter values are collected in Table I.

The shallower left well and the deeper right well hold 11 localized levels each. Contrary to the 3d system, the highest level in each well shows noticeable tunneling leakage to the other well. Furthermore, all levels above the barrier are delocalized. We use the lowest 38 of the high-lying levels together with the 22 localized ones to construct a 60-level system, which produces converged results in our simulations. This 1d potential with its energy levels is plotted in Figure 1a, where it is compared with the reaction-path profile, more precisely the vibrationally adiabatic potential along the reaction coordinate, and the $J = 0$ energy levels of HCN/HNC.

The 60-level system to some extent represents a 1d analogon of the HCN/HNC 550-level system. The analogy becomes most apparent when the comparison is made with the quasi-1d (reaction path-) 50-level system composed of the "reaction path states" (24 HCN and HNC bend states plus 26 of the delocalized states forming a network strongly coupled to the two bend progressions). In Figure 1b levels belonging to this set are highlighted as the longer lines.

It has already been noted in part I that in the optimization of few-cycle pulses for maximum population transfer, close agreement is found between the results of the 3d and 1d systems. Nevertheless, the 60-level system is not intended as a 1d model of the HNC→HNC isomerization nor as a fit to the reaction path potential. Indeed there are obvious differences between the 1d and 3d systems, which are also apparent in Figure 1. In particular, the shapes of the wells are different, and reflection at the sloped quartic wall replaces the quasi-reflection at the symmetry elements of the periodic 3d reaction-path potential. Our understanding of the 1d system is that of a more general model for population transfer in

many-level double well systems.

Noting that the width of the Fourier spectra renders state specific processes unlikely, the dynamics are analysed in terms of groups of states. For the 3d system we use the groups already defined in part I, i.e. "HCN" and "HNC" states as the levels below the barrier localized in the corresponding wells, and "high-lying" states above the barrier. In view of the analysis in terms of 1d wavepacket motion, these groups are partitioned into quasi-1d and non-1d subgroups: HCN and HNC into "bend" and "non-bend" states, the high-lying states into the quasi-1d "delocalized" and "localized high-lying" states without counterpart in a 1d system, which are further split into "HCN*" and "HNC*.

In the 1d system, we label the states in the right well as "R" (for reagents), the target product states in the left well as "P", and the states above the barrier as "delocalized"; these groups correspond to the HCN, HNC and delocalized states of the 3d system.

As in part I, the HCN bend level (0,16,0) is used as initial state for the 3d simulations. Its analogon in the 1d system is the 14th level (in energetic order), which is the eighth R-state. It is also connected to the lowest delocalized state via a four-quantum transition.

B. Pulse pairs

We use laser fields consisting of two single-lobe half-cycle pulses. The shape of the individual pulses is not essential as long as a scaling law for the fluence is maintained. As a simple tool for the purpose of analysing the dynamics we use cosine lobes with given amplitude A and length L, where $L = T/2 = \pi/\omega$, where T and ω are respectively the optical cycle and the carrier frequency. The half width at half height of these pulses is then $\alpha = T/3$. For the pulse pairs the delay time Δt is measured from peak to peak, and the clock time t is aLSO set to zero at the center of the pump pulse. The two pulses are indexed by 1 and 2, and we allow the individual variation of A_i and L_i, so that in the case of non-overlapping pulses the laser field takes the form

$$E(t) = \begin{cases} A_1 \cos(\pi t/L_1) & -L_1/2 \le t \le L_1/2, \\ A_2 \cos(\pi(t-\Delta t)/L_2) & -L_2/2 + \Delta t \le t \le L_2/2 + \Delta t, \\ 0 & \text{elsewhere.} \end{cases} \tag{2}$$

The extension to overlapping pulses is straightforward. The signs of the field lobes are

absorbed into the amplitudes A_i, which may thus be of arbitrary sign.

More suitable pulse forms for experimental setups, e.g. effective gaussian half-cycle pulses constructed as in part I, can be substituted in Eq. 2. Provided the fluence is scaled appropriately, there are only minor differences in the results. Of some interest for a laboratory setup should be the case of equal pump- and dump pulses, i.e. $L_1 = L_2$ and $A_1 = \pm A_2$. Sample simulations using such a setup show no sizable changes compared to results obtained with Eq. 2. The constraint to equal shape parameters generally only reduces the transfer probabilities by a few percent.

III. POPULATION TRANSFER IN THE 1D DOUBLE WELL SYSTEM

A. The pump-dump signal

Figure 2 gives an overview over the pump-dump transfer probabilities obtained for the 1d model system. The individual curves, which in the following will be denoted "signal curves", show P_{T} against Δt for all different sign combinations of the pump-and dump fields, and for different combinations of pump- and dump pulse widths. Our reference results are the ones presented in the middle panels, with pump- and dump- pulses of equal lobe lengths $L_1 = L_2 = 19.4$ fs. With this choice the peak-to-peak separation for a pair of exactly adjoining lobes is also 19.4 fs, and such a configuration corresponds to the optimum effective one-cycle pulses presented in part I. [1]

Concentrating first on the reference results, the four curves are characterized by a common pattern. Sizeable population transfer occurs in a time window with a width of about 15 fs, embedded into a recurrence structure with a recurrence time of about 66 fs, and considerable damping and broadening. The peak height is reduced to 50% at the first recurrence, and irregularities indicating the onset of sizeable interferences are visible right after the first recurrence. In fact as shown in Figure 3, already at the third recurrence the signal has broadened over the entire recurrence period and has a rich irregular substructure. We will return to this point below.

There are also some distinct differences between the four cases, concerning the optimum time delays and the amount of population transfer. Most notably the optimum time delays are all different for the four sign combinations of the pump- and dump fields. The shortest

delay, with Δt =19.4 fs, is found for a positive pump- and a negative dump field. This configuration corresponding exactly to a continuous effective one-cycle pulse with positive first lobe. The maximum transfer probability is just above 40%.

For a positive dump pulse there is an extra time delay of 18 fs, and for a negative pump pulse we observe an additional shift in the optimum time delay of about 17 fs. These shifts are independent of each other, so that the $-+$ field combination has an additional shift of 35 fs corresponding to $\Delta t \approx 55$ fs. Apart from the extra time shift, there are no significant differences between the $+-$ and $++$ combinations, while for negative pump fields the transfer probabilities are smaller, reaching only about 30%.

The graphs in the outer panels in Figure 2 show the effect of individually varying the widths of the pump pulse (left panels) and the dump pulse (right panels). While in both cases switching to shorter pulses has no sizable effects, the results for using longer pulses, as shown in the figure, indicate that the width of the *pump* pulse is a decisive parameter for the dynamics. It is strikingly appearent that for negative pump fields an increase of L_2 to 29 fs leads to a complete quenching of population transfer. Conversely, increasing the length of the *dump* pulse has no effects on the dynamics.

Small variations in the recurrence times with the sign and width of the pump pulse are due to the differences in the energy expectation values of the wavepackets prepared in the pump step, and indicate the energy dependence of the effective vibrational period in the anharmonic potential.

The vertical lines in Fig 2 denote the delays for which $+-$ or $-+$ field combinations result in continuous one-cycle pulses. Their relation to the peak positions makes clear why only a continuous pulse starting with a positive lobe can drive the transfer and thus explains the sign dependence and the outstanding role of the CEP reported in part I [1], which has to attain a value close to $\pi/2$. The larger delay required for a $-+$ lobe combination ($\Delta t \approx 37$ fs) would make the first lobe in an effective one-cycle pulse so long, that it could no longer carry out its pump function.

B. wavepacket motion

In order to obtain a deeper understanding of the findings in the previous subsection, we will now inspect the time evolution of the wavepackets that are prepared by the pump

pulses. Since evidently their dynamics depend on the sign of the pump field, we compare the two wavepackets induced by positive and negative pump pulses. We use the reference pulse width, i.e. $L_1 = 19.4$ fs.

In Figs. 4 and 5, selected frames of the two "wavepacket movies" are shown, which visualize the coordinate space motion in the potential. We show the density $\Psi_*(x;t)\Psi(x;t)$ of the wavefunction Ψ, with the baseline put at the energy expectation value $|\epsilon(t)|$. During the action of the pump pulse, both for a positive and a negative field the initial wavefunction (frame 1 in both figures) is lifted to a higher energy, without much change of its shape (frame 2). Although due to the broad frequency spectrum of the pulse the anharmonicity in the well plays no role and levels below and above the initial state are populated at equal rates, the net result is an increase in energy due to the much larger available phase space above the initial state, which includes the delocalized levels.

Immediately after their preparation, the wavepackets arising from differently directed pump fields experience different fates. This sign-dependence can be understood by an energy shift that raises or lowers the potential by the energy $|\mu(R)x|$. With the dipole moment negative in the right well and positive in the left one, a positive pump pulse raises the potential at the reagent side and the extra force provides the newly formed wavepacket with an acceleration towards the barrier, where it just arrives by the end of the pulse (frame 3 in Figure 4). Conversely a negative pump pulse accelerates the wavepacket towards the outer repulsive wall (frame 3 of Figure 5), so that before moving towards the barrier it must complete a vibrational half-period in the reagent well before going on to reach the barrier (frame 4 of Figure5). This leads to the observed extra delay of around 17 fs. In both cases the more energetic parts of the wavepacket traverse the barrier to reach the target well, where they may eventually be de-excited by the dump pulse.

The action of the dump pulse can be rationalized in a similar way. When the wavepacket has crossed the barrier and moves towards the left repulsive wall, then due to the interaction with the now positive dipole only a negative field will apply a decelerating force, which causes the dump into the target well (frame 4 of Figure 4, frame 5 of Figure 5). A positive dump field must await the change of the direction of wavepacket motion; it can only become effective after reflection of the wavepacket at the left repulsive wall (frames 5 and 6, respectively, for the two cases), and the completion of a vibrational half-cycle in the target well (frames 6 and 7, respectively). This adds the extra contribution of 18 fs to Δt. The remaining frames show

the completion of the full recurrence cycle up to the first re-arrival at the dumping-zone.

Since the wavepacket has components both in the well and above the well, there are two different, but strongly coupled modes of motion with very different individual recurrence times. The interplay and the interferences between the two modes gives rise to the quick decay of the recurrence structure noted in the previous subsection.

We now turn to the question why a successful negative pump pulse must not be too long. This effect has its origin in the reflection of the wavepacket at the right repulsive wall, which occurs about 10 fs after the formation of the wavepacket. If the negative pump field is still "on" while parts of the wavepacket already travel back towards the barrier, the wavepacket motion will be decelerated, effecting a dump to the reagent well states. This can be understood as a destructive interference or, phenomenologically, as an internal pump-dump process within a single field lobe.

It is interesting to note that this situation exactly corresponds to the one described by Korolkov et al. [13] for the excitation of a diatomic molecule by half-cycle pulses. They describe dissociation of the molecule by a positive half-cycle pulse, but a continuous pump-dump process to high-lying vibrational states via continuum states without dissociation upon a sign change of the field. With their choice of dipole function, a positive lobe prepares a wavepacket accelerating and moving away from the repulsive wall, corresponding to an elongating molecule that goes on to dissociate. Conversely, a negative field produces a wavepacket heading towards the repulsive wall. With the pulse still on after reflection, the molecule is de-excited to bound states. This suggests that the asymmetry in the dissociation probability should vanish upon employing shorter half-cycle pulses.

IV. POPULATION TRANSFER IN THE 3D HCN/HNC SYSTEM

A. The pump-dump signal

Figure 6 gives an overview over the pump-dump isomerization probabilities obtained for the 3d system. The plots are analogous to those for the 1d model system in Figure 2, except that the variation in the pulse width is now towards shorter pulses rather than towards longer ones. The reason for this will become clear in the discussion. The Figure demonstrates that the pattern of the recurrent 1d wavepacket dynamics is indeed found in

the results for the HCN/HNC system, albeit with some slight differences in quantitative terms. More importantly however, there are also features without a counterpart in the 1d system, which will be seen to be peculiar to higher-dimensional potentials.

The similarities and differences are most readily appearent by superimposing the 3d signal curves onto those for the 1d 60-level system. In Figure 7 this is done for the case $L_1 = L_2 = 9.7$ fs. Note in order to facilitate the comparison we use shorter pulses, since this gives rise to increased transfer probabilities and to better comparability for the case of negative pump pulses. Both systems show signals peaking near 40% transfer probability, a recurrence structure with almost equal recurrence times, similar extra time delays for the different sign combinations of the fields, and some degree of quenching when the pump field is negative.

Small differences in the numerical values are irrelevant in view of the fact that the 1d system represents no formal fit to the 3d system. Thus in the 3d system a recurrence time of about 60 fs is observed, with small variations depending on the pump-pulse dependent average energy of the traveling wavepacket, compared with ≈66 fs in the 1d model. Similarly, there are some noticeable differences in the sign-related spacings; e.g. the offset between the peaks for negative and positive dump pulses is shorter in the 3d system by about 5 fs. This effect can easily be rationalized by considering the difference between the right-hand repulsive wall of the 1d system and the right-hand refecting wall of the 3d system in Figure 1. Another difference concerns the quenching of the pump-dump process with increasing pump-pulse width. Figs. 6 and 7 show that in the HCN/HNC system the signals for negative pump fields diappear upon increasing L_1 from 9.4 to 19.4 fs. In the 1d model the pulses may be somewhat longer: here the same phenomenon occurs around 24 fs.

However, a much more striking difference, which goes beyond the qualitative features related to a (quasi-) 1d wavepacket motion, is the pronounced secondary peak in P_{HNC}. For the $+-$ combination of pump- and dump pulses is observed about 21 fs after the main peak, and it is most prominent in the middle panels of Figure 6. The peak is equally present for the $-+$ combination, whereas no trace of such a feature is seen for positive dump fields. This suggests that the additional peak is strongly linked to the dump pulse. Indeed upon reduction of L_2 to 9.7 fs (right panels of Figure 6 and Figure 7), the secondary peak becomes less pronounced; it disappears altogether if L_2 is further reduced to 5 fs.

Summing up, indications from the results with continuous one-cycle pulses in part I

and the comparison in Figure 7 suggest that by and large the well-to-well transfer in the 3d system proceeds as a quasi-1d process along the reaction coordinate. However, an additional mechanism is present in the 3d system, most clearly borne out by the secondary peak in the pump-dump signals arising for positive pump fields. The origin of this peak, as well as other related aspects of the 3d system, will be discussed in the following subsection.

B. One-dimensional and three-dimensional transfer mechanisms

In order to quantify the notion of a quasi-1d mechanism, it is useful to partition the populations into the quasi-1d and non-1d contributions defined in Section IIA. For the +− field combination, in Figure 8 we show the partitioning of P_{HNC} into bend- state contributions, which are representative for the reaction coordinate, and non-bend state contributions, which arise from processes orthogonal to the reaction coordinate. The sub-populations depend on the time delay and the pulse widths. At the main peak the HNC bend levels are indeed predominantly populated, in accord with the quasi-1d interpretation of the dynamics. Note in particular that the bend states occupy less than 20% of the phase space of HNC states, so that the population ratio of about 2:1 in favor of bend states indicates a strong propensity for the latter, and thus effectively a 1d process.

The argument can be strengthened by considering the population dynamics during the pump and dump steps. Figure 9a demonstrates that the wavepacket prepared by the pump pulse (shown is our standard positive pump field with $L_1 = 19.4$ fs) has almost negligible contributions from non-bend HCN states and localized high-lying states, indicating a process strongly analogous to wavepacket formation in the 1d system. In Figure 9b we show the evolution of the populations during a negative 19.4 fs dump pulse corresponding to the main peak of the signal curve ($\Delta t = 19.4$ fs). Initially the transition leads from delocalized states to HNC bend states, again a quasi-1d process. Non-bend states are populated only during the later parts of the dump pulse by internal redistribution among the HNC states. Incidentially, at the same time the same type of redistribution occurs among the HCN states.

Returning to Figure 8, a marked propensity for dumping to HNC non-bend levels is found for the secondary peak near $\Delta t = 40$ fs. The lower panels show that at the secondary peak a reduction of the pulse length leads to a rapid decrease of the non-bend contributions, and eventually to a complete disappearance of population transfer. Let us also note that the

HNC levels populated are all of the form $(1, v_2, 0)$, i.e. the NH stretch mode is excited.

At the secondary peak, isomerization can be described as a pump-pump-dump process, where the additional pump step and the dump are both mediated by the second (i.e., the "dump") pulse. Grossly this mechanism of population transfer can be deduced from the time-evolution of the energy expectation value $< \epsilon >$, as demonstrated in Figure 10 for various pulse configurations. The pump-dump character of the isomerization at the main peaks of the $+-$ and $++$ field combinations is clearly reflected in the increase of $< \epsilon >$ during the first pulse and its decrease during the second one. In contrast, at the secondary peak an additional pump process raising the energy is observed in the initial stages of the second pulse, immediately followed by a dump process decreasing the energy. If the pulse is too short, the dump process is terminated before states below the barrier are reached.

Initially the second pump process is independent of the delocalized part of the wavepacket. The primary pump action is on the localized part of the wavepacket, which travels in the HCN well and has completed its first vibrational cycle. Its most energetic components penetrate close to the barrier crest, where some overlap exists with localized, but highly excited HNC states above the barrier. The pump part of the second pulse excites just such states off the 1d reaction coordinate. This is visualized in Figure 11a, which shows the detailed population dynamics occurring in a 19.4 fs negative "dump" pulse corresponding to the secondary peak of the signal curve. Partitioning the high-lying localized states into the subgroups of HCN* and HNC* states, it is seen that in the first part of the pulse population switches from HCN bend states to HNC* states.

The newly formed energetic wavepacket interacts with the "original" delocalized wavepacket, which is about to reach the barrier from the side of the product well. This interaction adds a component of motion orthogonal to the reaction coordinate, and modifies the wavepacket such that population can immediately be dumped into the HNC well. This becomes evident by scanning the time window of Figure 11a with shorter pulses, as in Figure 11b and c. Placed near $\Delta t = 36$ fs, corresponding to the initial parts of the dump pulse of Figure 11a, a 5 fs probe pulse effects a clean excitation from HCN bend to HNC* states. However, if the probe pulse is applied about 4 fs later (marked B in Figure 11), the wavepacket in the HCN well has left the barrier zone. The population now switches from the HCN bend states to delocalized states and to HCN non-bend states, and no population is dumped to HNC well states. Yet at the same time the dump process proceeds efficiently

with the modified wavepacket.

Localized high-lying states, which appear to be essential for the mechanism described above, have no analogon in 1d double wells. Hence the pump-pump-dump mechanism ascribed to the secondary peak should be specific to higher dimensional systems.

Since the pump-pump-dump mechanism involves wavepacket motion in the HCN well, it has its own recurrence time, approximately, but not exactly, half the recurrence time of the large- amplitude delocalized motion responsible for the main pump-dump mechanism. The participation of two coupled recurrent motions has already been noted in the 1d case, where it leads to the rapid degradation of the signal peak. With two different recurrences now directly contributing to the signal in the 3d system, a composite peak pattern arises. Peaks may be hidden or turned into shoulders, and in conjunction with inevitable interferences the signal curves attain a complicated appearance.

In Figure 12 we show the signal curve obtained with 19.4 fs pulses in the $+-$ configuration over a longer interval of Δt. The graph is analogous to its counterpart for the 1d system in Figure 3. Based on the assumption of two independent recurrence times and on the propensities for bend- or non-bend product states, a tentative assignment of various peaks and shoulders in the signal function is indicated. The assignment is not fully conclusive, and in any case from the third recurrence onwards it becomes meaningless in view of the prevalence of interference effects.

V. SUMMARY AND CONCLUSIONS

The following findings apply to population transfer in double well potentials induced by pairs of time-delayed half cycle pulses:

Population transfer across the barrier can be achieved with a pump-dump strategy via high-lying delocalized states. The transfer is mediated by the wavepacket prepared by the pump pulse, which is a superposition of localized states in the reagent well and delocalized states above the barrier. Its delocalized, high-energy component traverses the barrier and can be dumped to states in the product well. The underlying large-amplitude motion across both wells gives rise to a recurrence structure with a period distinctly longer than those for localized motion in the wells. In 3d systems, wavepacket formation and motion are also (quasi-) 1d; e.g. in the case of molecular isomerization, wavepacket motion and population

transfer proceed along the reaction coordinate.

There are several peculiarities to the setup, which modify the usual behavior of pump-dump processes. First, two different, but strongly coupled constituents of wavepacket motion are present, one proceeding locally in the reagent well and another one involving large-amplitude motion across both wells. Their different, and in general non-commensurate time scales together with strong interferences give rise to irregularities and to fairly rapid degradation of the recurrence structure.

Second, the signs of the pump- and dump fields become decisive parameters. The sign of the pump field together with the sign of the dipole function determines the direction of motion of the nascent wavepacket. If this initial motion is directed away from the barrier, then the ensuing additional half-period of wavepacket motion in the reagent well gives rise to an extra time delay for the principal peak of the signal curve. Similarly, the sign of the dump field determines whether the deexcitation to product states occurs while the wavepacket motion across the product well is towards the repulsive wall or towards the barrier. The latter case again gives rise to an extra time delay, so that the signal curves for the four possible sign combinations of the pump- and dump pulses are all different: they are characterized by different peak positions, but a common recurrence time. The most efficient setup is the one with no extra delays, since damping is absent in this case. In the present example this is the combination of a positive pump- and a negative dump pulse, and the timings are such that the required sequence can also be generated by a continuous $-$sine like effective one-cycle pulse.

Third, the duration of a pump pulse inducing motion of the nascent wavepacket towards the repulsive wall must be sufficiently short. If the pulse is still "on" while the wavepacket is already reflected and moves back towards the barrier, then the wavepacket will be annihilated by destructive interference, in what may phenomenologically be described as a "continuous pump-dump process" [13], and population transfer will be quenched. In HCN/HNC, the critical pulse length is found to be about 10-15 fs. Note however that this time scale argument will hold more generally; it should also apply in single well systems, e.g. in the dissociation of a diatomic molecule. [13]

This internal quenching mechanism aloso explains why continuous effective one-cycle pulses with a +sine shape cannot drive HCN$\rightarrow$HNC isomerization, and why population transfer with effective one-cycle and sub-one cycle pulses is so extremely sensitive to the

CEP. [1]

In the 3d system, in addition to the basic quasi-1d wavepacket motion and its associated peak- and recurrence pattern, there is room for additional "higher-dimensional" mechanisms. Specifically in the 3d HCN/HNC system, for certain pulse configurations we identified a pump-pump-dump mechanism associated with wavepacket motion in the reagent well and with population transfer to partially stretch-excited states off the reaction coordinate, which gives rise to a secondary peak in the signal curve.

Finally we want to repeat our point that although the present results are obtained using simple separately adjusted cosine lobes, very similar results are obtained with pairs of identical cosine half-cycle pulses under an envelope, either two very closely spaced pulses of different sign, or two pulses of equal sign with an extra time delay.

Acknowledgments

This work was sponsored by the Austrian Science Fund within the framework of the Special Research Program F016 "ADLIS".

---

[1] C. Uiberacker and W. Jakubetz, preceding paper.

[2] W. Jakubetz and B. L. Lan, Chem. Phys. **217**, 375 (1997); W. Jakubetz, Faraday Discuss. **113**, 355 (1999).

[3] S. P. Shah and S. A. Rice, Faraday Discuss. **113**, 113/15 (1999); S. P. Shah and S. A. Rice, J. Chem. Phys. **113**, 6536 (2000).

[4] S. Chelkowski and A. D. Bandrauk, Chem. Phys. Lett. **233**, 185 (1995); H. Umeda, M. Sugawara, Y. Fujimura, and S. Koseki, Chem. Phys. Lett. **229** 233 (1994); V. Kurkal and S. A. Rice, Chem. Phys. Lett. **344**, 125 (2001).

[5] I. Vrábel and W. Jakubetz, J. Chem. Phys **118**, 7366 (2003).

[6] R. Kienberger, M. Hentschel, M. Uiberacker, Ch. Spielmann, M. Kitzler, A. Scrinzi, M. Wieland, Th. Westerwalbesloh, U.Kleineberg, U. Heinzmann, M. Drescher, and F. Krausz, Science **297**, 1144 (2002).

[7] A. H. Zewail, *Femtochemistry*, edited by J. Manz and L. Wöste (VCH, Weinheim, 1995), Vol. 1, p.15.

[8] D. J. Tannor and S. A. Rice, J. Chem. Phys. **83**, 5013 (1985); D. J. Tannor, R. Kosloff, and S. A. Rice, J. Chem. Phys. **85**, 5805 (1986);

[9] T. Brabec and F. Krausz, Rev. Mod. Phys. **72**, 55 (2000);

[10] J. Manz, in *Femtochemistry and Femtobiology: Ultrafast Reaction Dynamics at Atomic Scale Resolution*, edited by V. Sundström (Imperial college Press, London, 1997), p. 80.

[11] P. Dietrich and P. Corkum, J. Chem. Phys. **97**, 3187 (1992); L. V. Keldysh, Soviet Physics JETP **20**, 1307, (1965).

[12] J. M. Bowman, B. Gazdy, J. A. Bentley, T. J. Lee, and C. E. Dateo, J. Chem. Phys. **99**, 308 (1993).

[13] M. V. Korolkov, J. Manz, and G. K. Paramonov, Chem. Phys. **217**, 341 (1997).

TABLE I: Parameters of the one-dimensional piecewise quartic double-well potential (all entries in au)

α_r	0.7575
α_l	1.1364
D_l	0.0640
D_r	0.0406
reduced mass	3.5
μ	-6.0

Figure captions

Figure 1. 1d and 3d double well potentials. (a) The 1d potential, eq.(1) and Table I, with the reagent (R) well to the right and the product (P) well to the left. The eigenenergies of the lowest 34 levels are indicated as horizontal bars. All levels above the barrier are delocalized. (b) Vibrationally adiabatic potential profile along the reaction coordinate of the 3d HCN/HNC potential energy surface of Bowman et al. [12] with the HCN well to the right and the HNC well to the left. The vertical lines are reflecting potential walls which transform the periodic reaction coordinate potential into an equivalent double well potential utilizing its reflection symmetry. The eigenenergies of the lowest $J = 0$ levels indicated as horizontal bars. Longer bars denote members of the quasi-1d 50-level system, where those in the wells are bend states $(0, v_2, 0)$. Localization and different degrees of delocalization are indicated by the horizontal placement of the bars. In both panels the very long bar in the right well denotes the standard initial state of the simulations, and the bold dotted horizontal line schematically indicates the motion of the delocalized part of the wavepacket formed by the pump pulse.

Figure 2. Pump-dump signal curves P_T vs. ΔT for the 1d 60-level system. Upper row, panels (a)-(c): Positive pump fields. Lower row, panels (d)-(f): negative pump fields. In all panels, full line denote negative dump fields, and dashed lines denote positive dump fields. Results in the central row, panels (b) and (e), are for the standard pulse length $L_1 = L_2 = 19.4$ fs. Panels (a) and (d): Increased pump pulse length ($L_1 = 29.0$ fs). Panels (c) and (f): Increased dump pulse length ($L_2 = 29.0$ fs). Thin vertical lines indicate the time delay for which the pump and dump pulses combine to a continuous one-cycle pulse.

Figure 3. Pump-dump signal curve for the 1d model system as in Figure 2b, but over a time range encompassing the first three recurrences.

Figure 4. Snapshots of the wavepacket prepared in the 1d model system by a positive pump pulse with length $L_1 = 19.4$ fs. Plotted is $\Psi_*(x,t)\Psi(x,t)$ at times t shown in the panels. The horizontal lines supporting the wavepacket indicate the average energy $< \epsilon(t) >$. Horizontal arrows show the direction of wavepacket motion. Vertical up arrows denote center of the initial pump, down arrows denote a possible successful dump by positive or negative pulse

lobes as shown as inserts.

Figure 5. Snapshots of the wavepacket prepared in the 1d model system by a negative pump pulse (as Figure 4).

Figure 6. Pump-dump signal curves for the 3d 550 level system representing HCN/HNC. Plot conventions are as in Figure 2, except for the pulse lengths in the outer panels; Panels (a) and (d): Reduced pump pulse length ($L_1 = 9.7$ fs). Panels (c) and (f): Reduced dump pulse length ($L_2 = 9.7$ fs).

Figure 7. Comparison of signal curves for the 1d and 3d systems. In panels (a)-(d), 1d and 3d curves are superimposed for pump- and dump pulse sign combinations as indicated. Pulse lengths are $L_1 = L_2 = 9.7$ fs in all cases.

Figure 8. Partitioning of the pump-dump signal curves into bend and non-bend contributions. All results are for the $+-$ sign combination of pump- and dump pulse, with pump pulse length $L_1 = 19.4$ fs. Panels (a)-(c) differ in the dump pulse length as indicated.

Figure 9. Group population dynamics in a typical pump-dump isomerization. Panel (a): Dynamics induced by a positive pump pulse with $L_1 = 19.4$ fs. Panel (b): Dynamics induced by a negative dump pulse with $L_1 = 19.4$ fs at the principal peak of the signal curve in Figure 6b. Thin full lines: HCN bend well states. Thin dashed lines: HCN non-bend well states. Medium full lines: delocalized states. Medium dashed lines: localized high-lying states. Bold full line: HNC bend well states. Bold dashed line: HNC non-bend well states. All full lines denote states participating in quasi-1d dynamics along the reaction path. Fields are schematically shown as inserts in the lower parts of the panels.

Figure 10. Evolution of the energy expectation value $< \epsilon >$ during pump-dump and pump-pump-dump processes, with the fields schematically shown as inserts below the energy curves. Thin line: Pump-dump process at the principal peak. Bold line: Pump-pump-dump process at the secondary peak. If the dump lobe length is reduced (dashed line), there is no dump to HNC products.

Figure 11. Group population dynamics in the pump-pump-dump process. Plot conventions

are as in Figure 9, except that the localized high-lying states are further partitioned into HCN* (thin short-dashed) and HNC* (bold short-dashed). Panel (a): Second pump step followed by a dump during the negative second pulse with length $L_2 = 19.4$ fs, at the secondary peak of the signal curve in Figure 6b. Panels (b) and (c): Scan of the time window in panel (a) with shorter probe pulses centered at delay times denoted A and B in panel (a).

Figure 12. Pump-dump signal curve for the 3d system analogous to Figure 3, with an assignment of the two overlapping recurrence structures of the delocalized large- amplitude motion (60 fs) and the localized motion in the HCN well (32 fs).

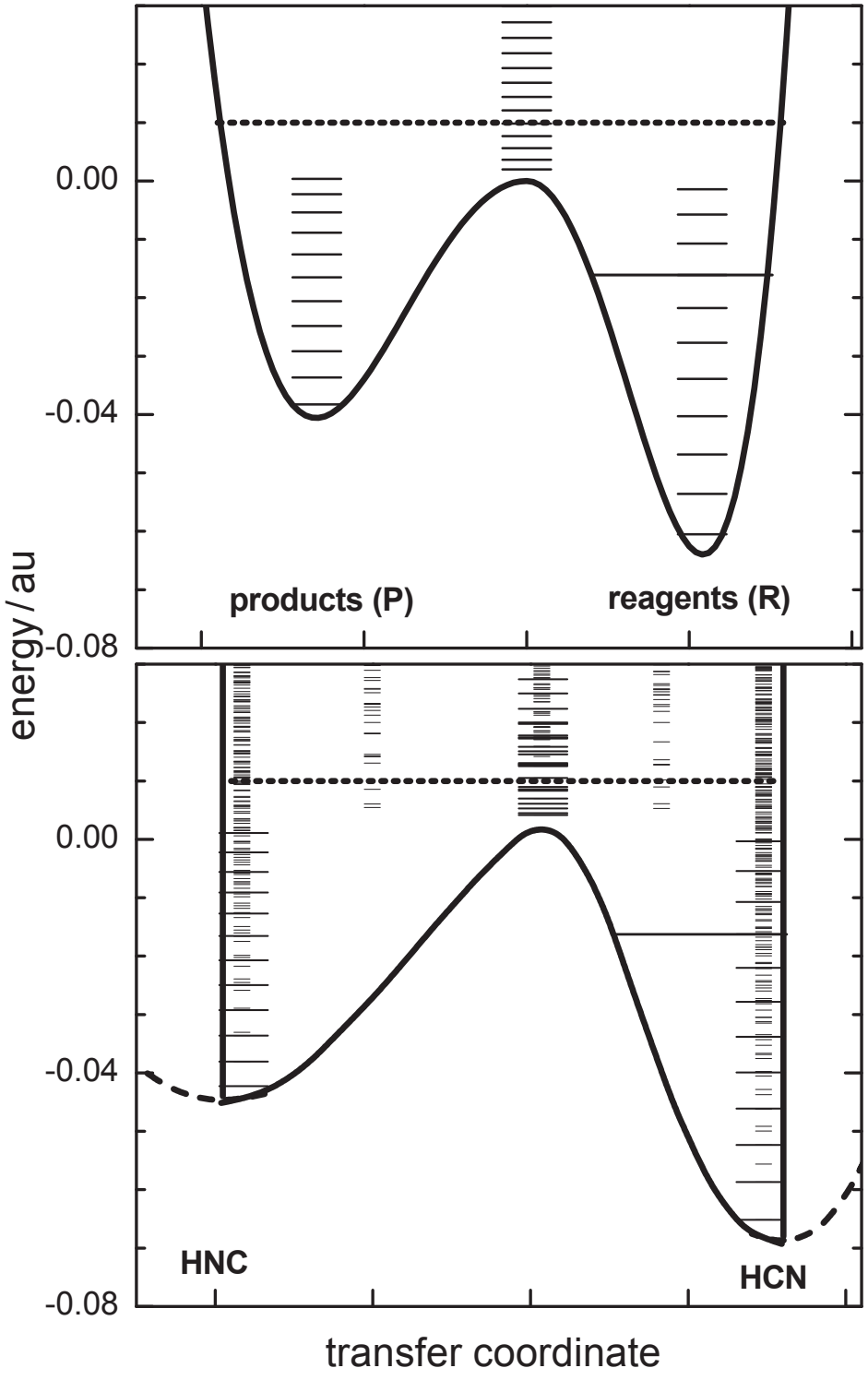
0.00
-0.04
-0.08
products (P)
reagents (R)
energy / au
0.00
-0.04
-0.08
HNC
HCN
transfer coordinate

FIG. 1:

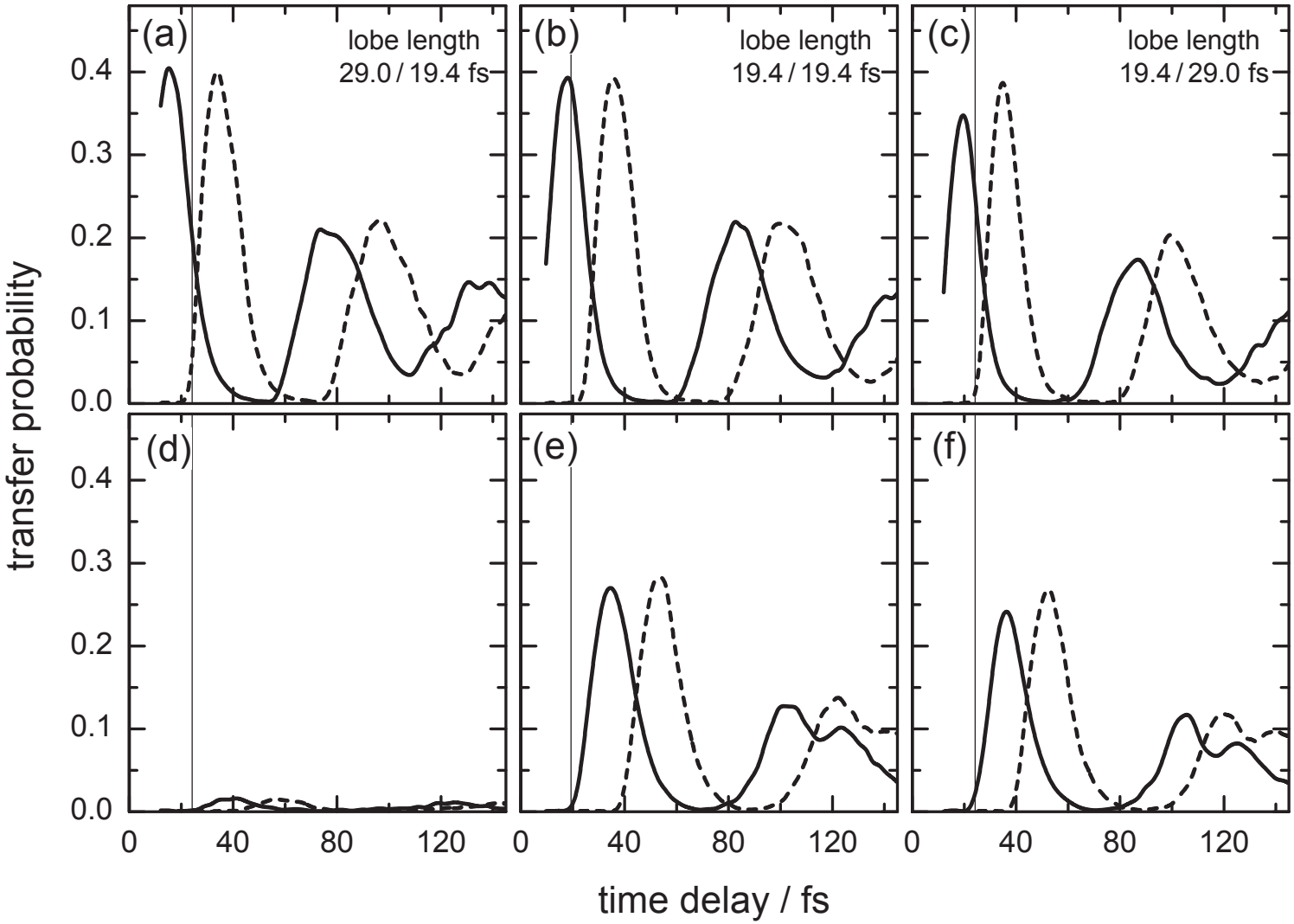
(a)
lobe length
29.0 / 19.4 fs
(b)
lobe length
19.4 / 19.4 fs
(c)
lobe length
19.4 / 29.0 fs
(d)
(e)
(f)
transfer probability
time delay / fs
0.0
0.1
0.2
0.3
0.4
0
40
80
120

FIG. 2:

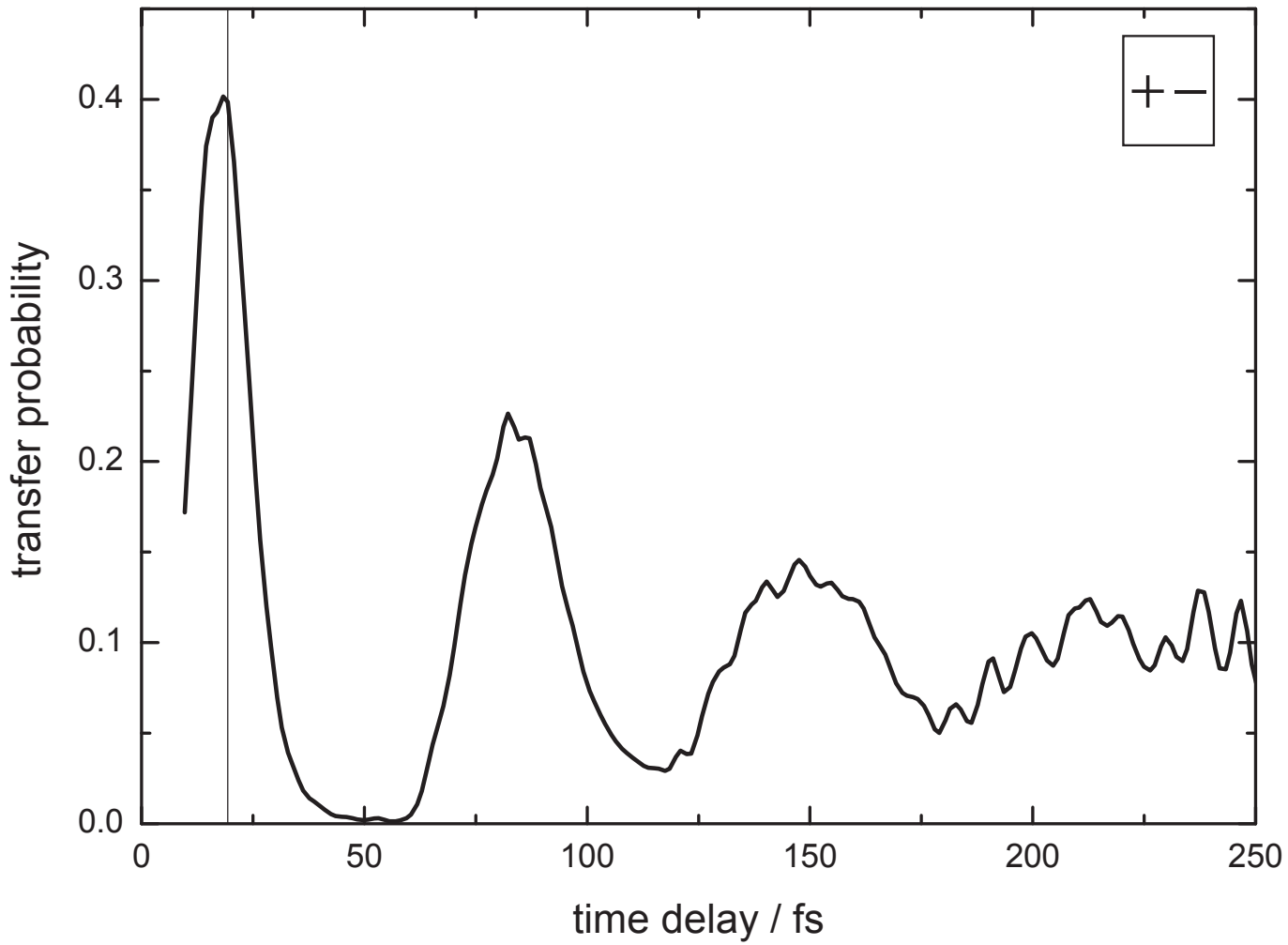
transfer probability
time delay / fs
0.0
0.1
0.2
0.3
0.4
0
50
100
150
200
250
+
−

FIG. 3:

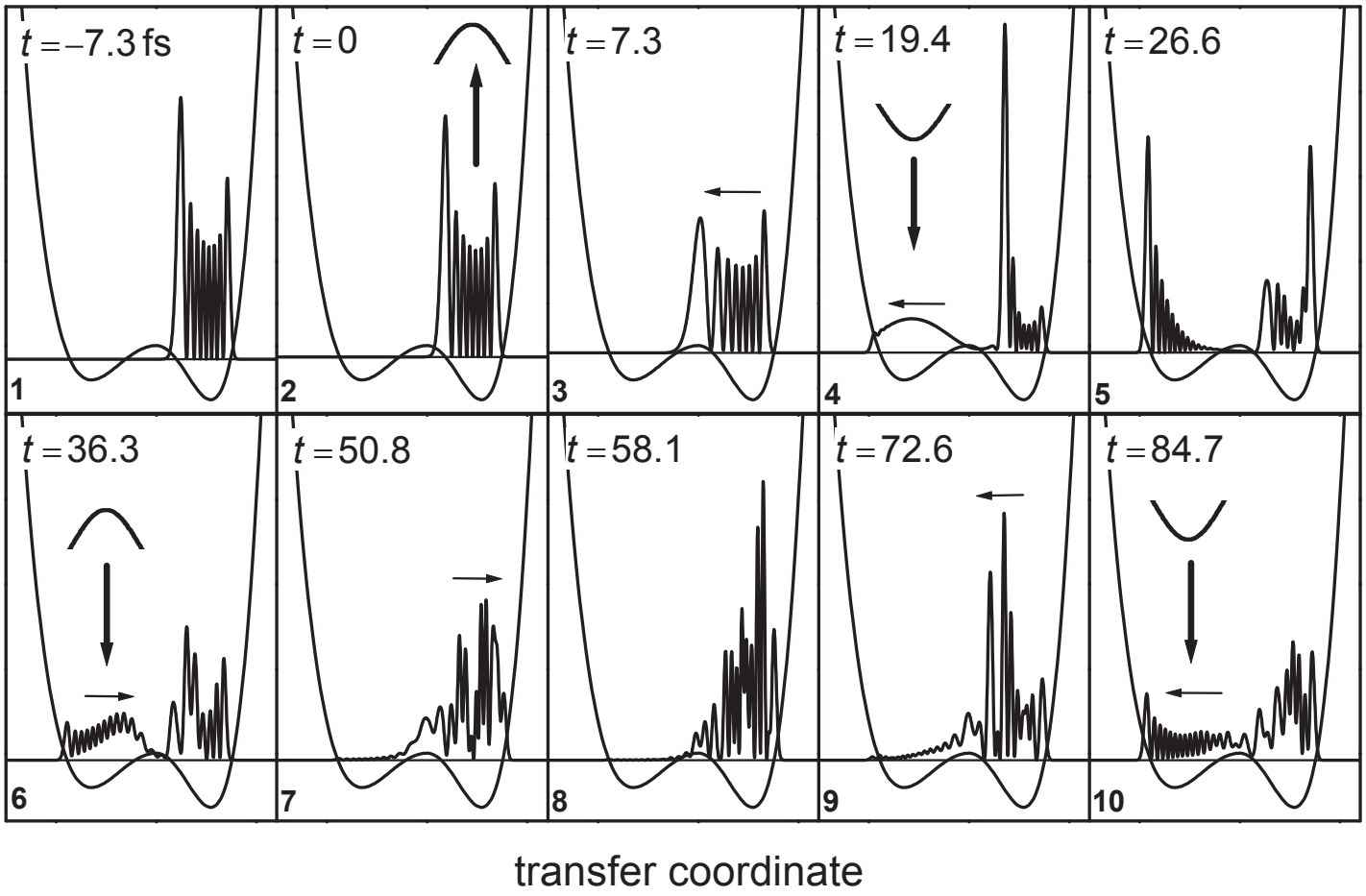
t = –7.3 fs
t = 0
t = 7.3
t = 19.4
t = 26.6
1
2
3
4
5
t = 36.3
t = 50.8
t = 58.1
t = 72.6
t = 84.7
6
7
8
9
10
transfer coordinate

FIG. 4:

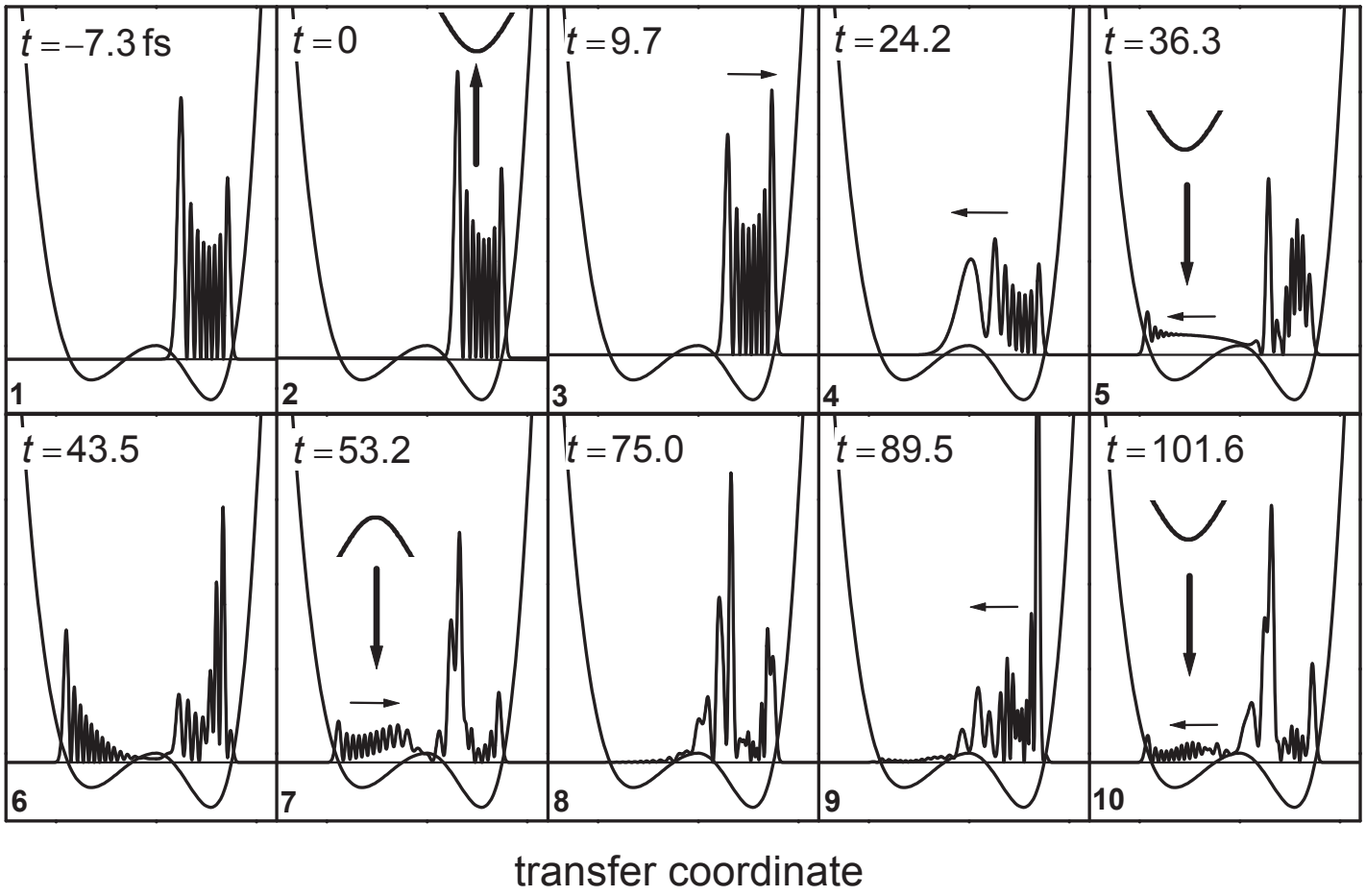
t = –7.3 fs
t = 0
t = 9.7
t = 24.2
t = 36.3
1
2
3
4
5
t = 43.5
t = 53.2
t = 75.0
t = 89.5
t = 101.6
6
7
8
9
10
transfer coordinate

FIG. 5:

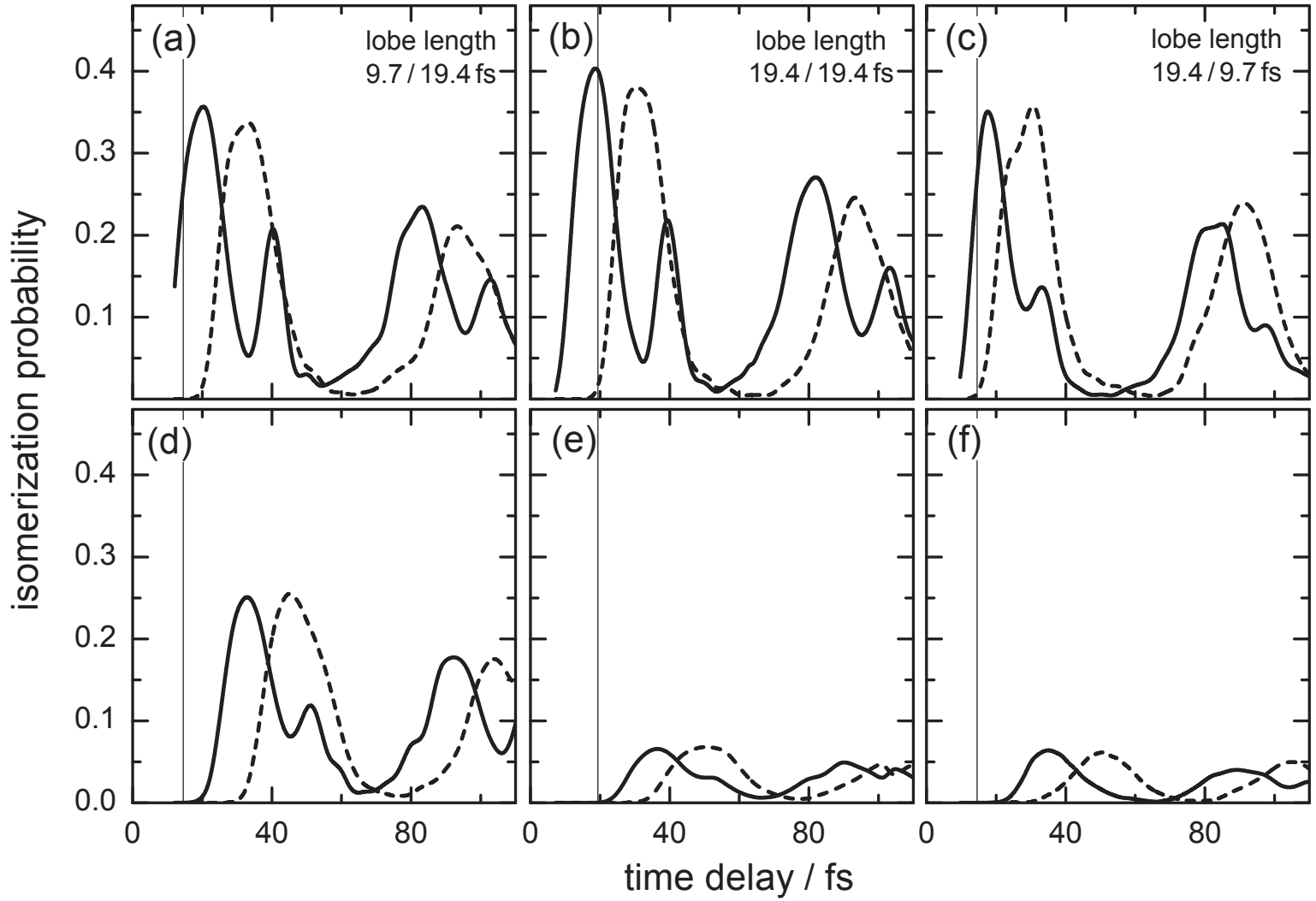
(a)
lobe length
9.7 / 19.4 fs
(b)
lobe length
19.4 / 19.4 fs
(c)
lobe length
19.4 / 9.7 fs
(d)
(e)
(f)
isomerization probability
0.0
0.1
0.2
0.3
0.4
0
40
80
time delay / fs

FIG. 6:

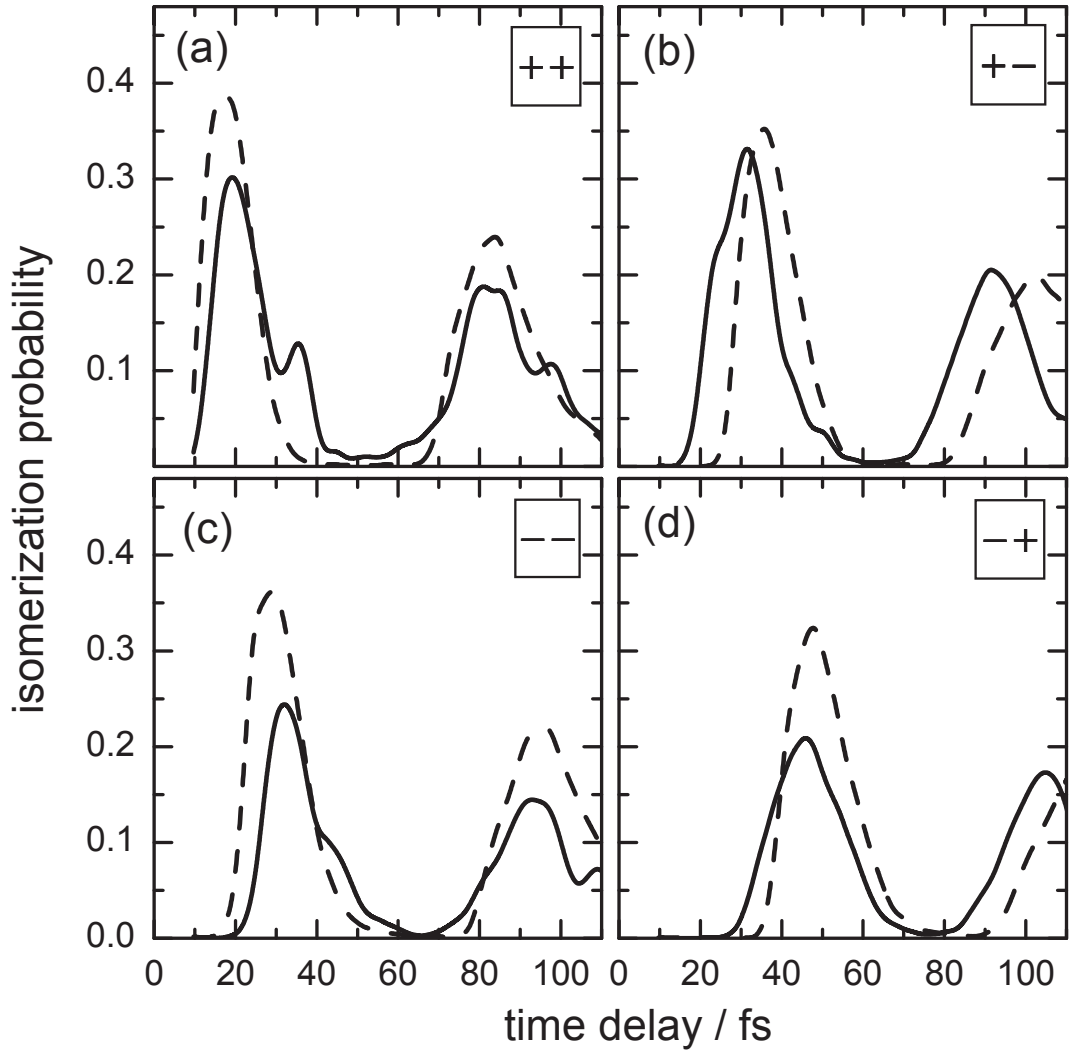
(a)
++
(b)
+−
(c)
−−
(d)
−+
isomerization probability
0.0
0.1
0.2
0.3
0.4
0
20
40
60
80
100
time delay / fs

FIG. 7:

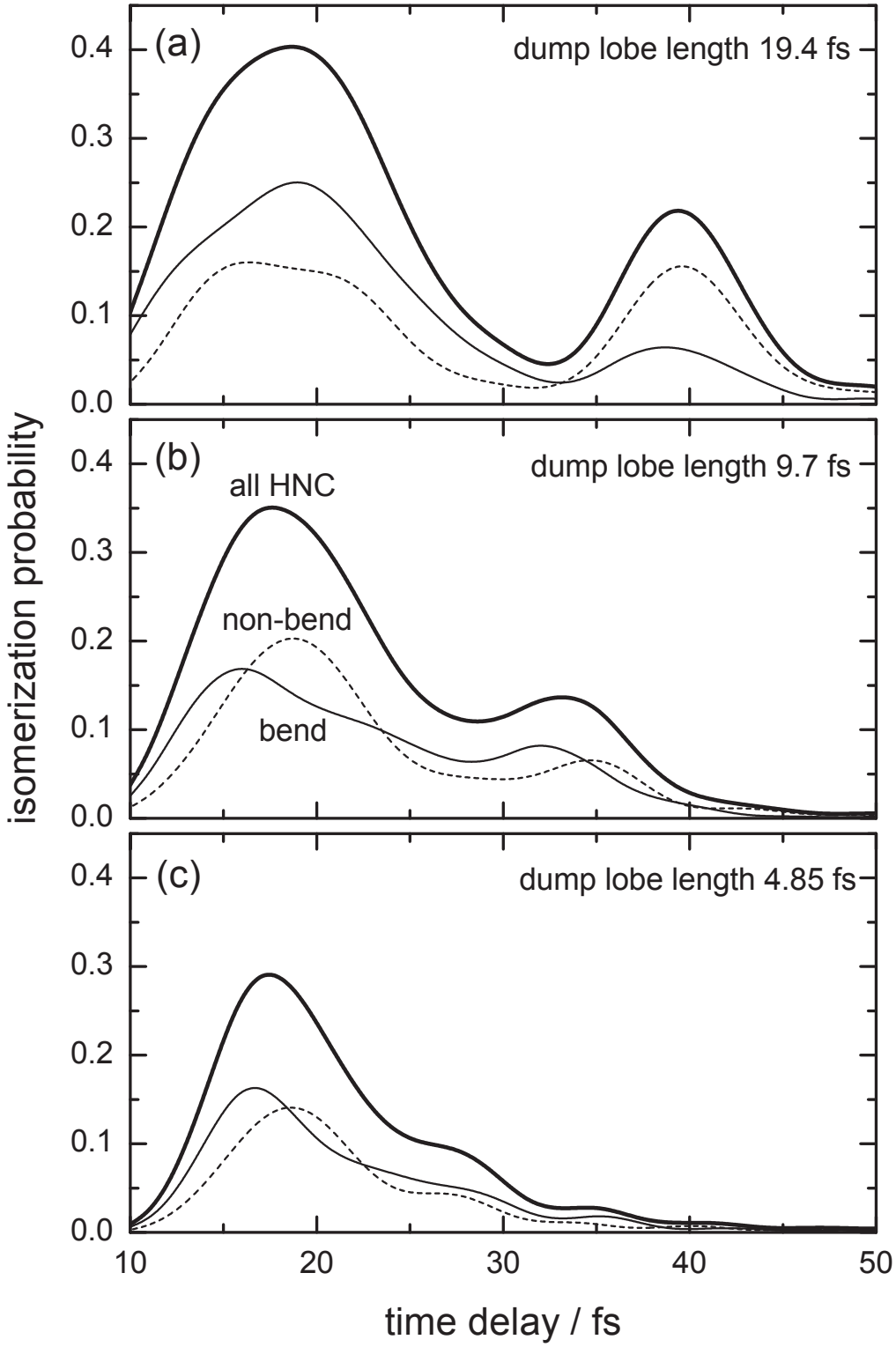
(a)
dump lobe length 19.4 fs
(b)
dump lobe length 9.7 fs
all HNC
non-bend
bend
(c)
dump lobe length 4.85 fs
isomerization probability
time delay / fs
0.0
0.1
0.2
0.3
0.4
10
20
30
40
50

FIG. 8:

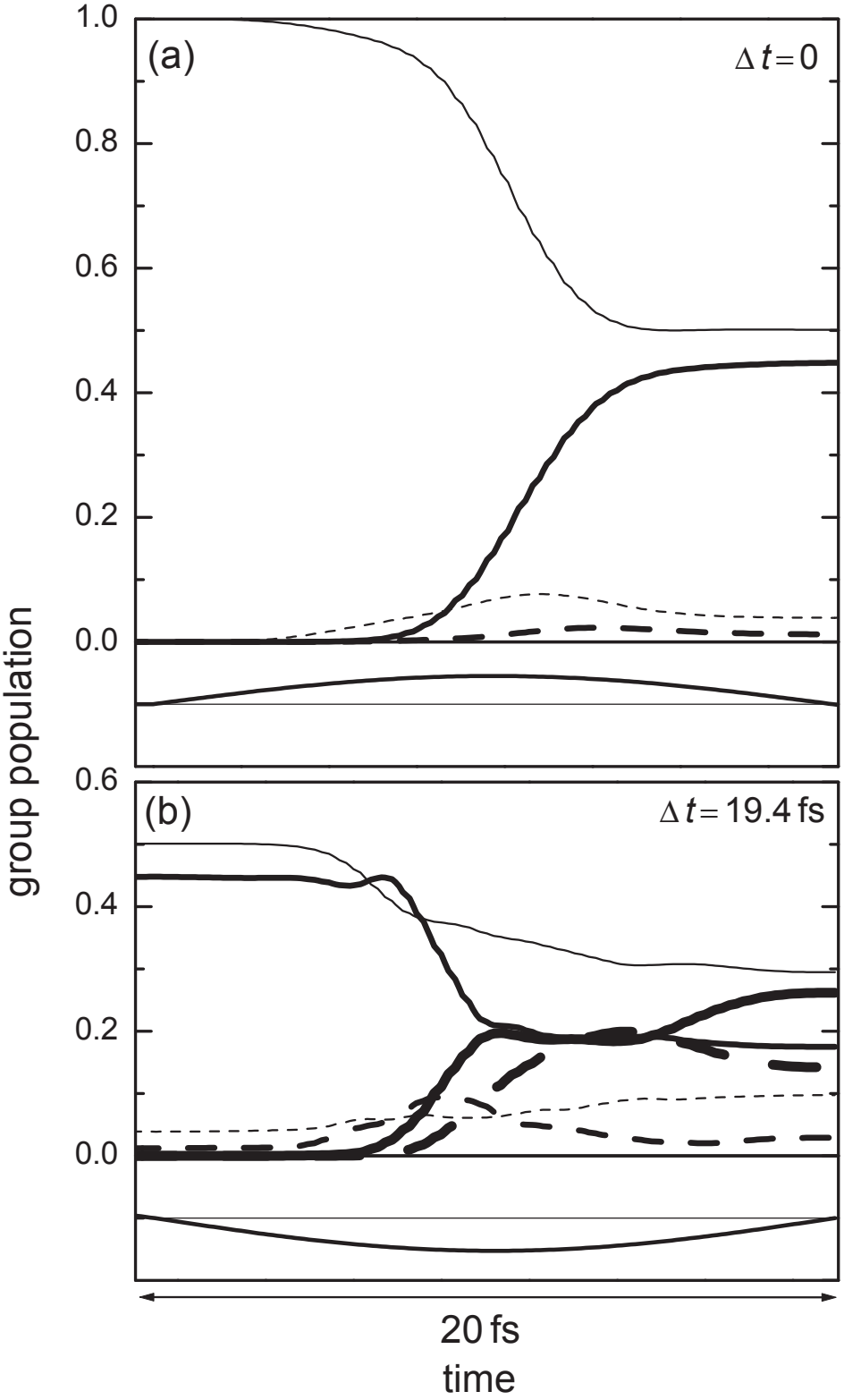
1.0
0.8
0.6
0.4
0.2
0.0
(a)
Δt = 0
0.6
0.4
0.2
0.0
(b)
Δt = 19.4 fs
group population
20 fs
time

FIG. 9:

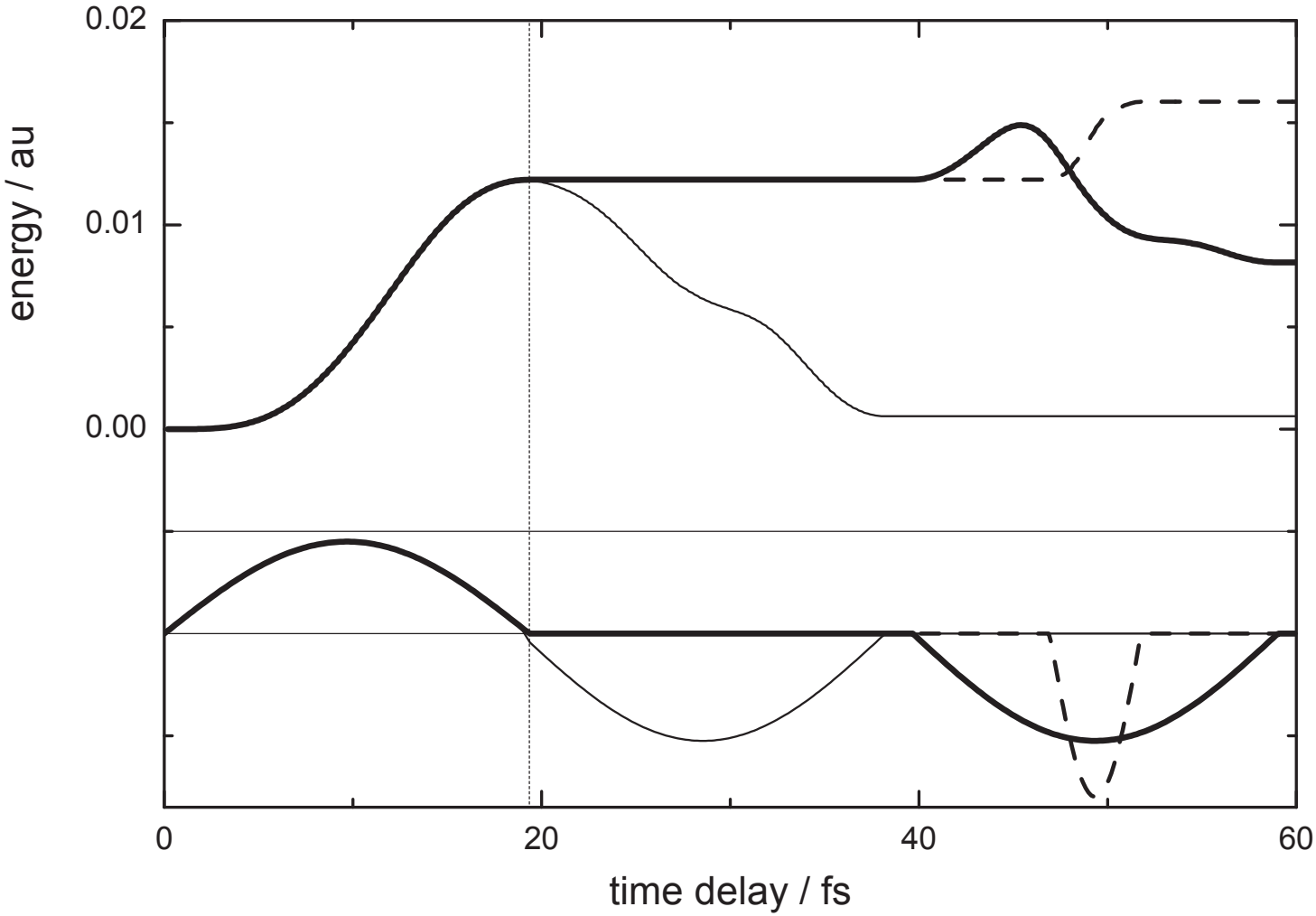

FIG. 10:

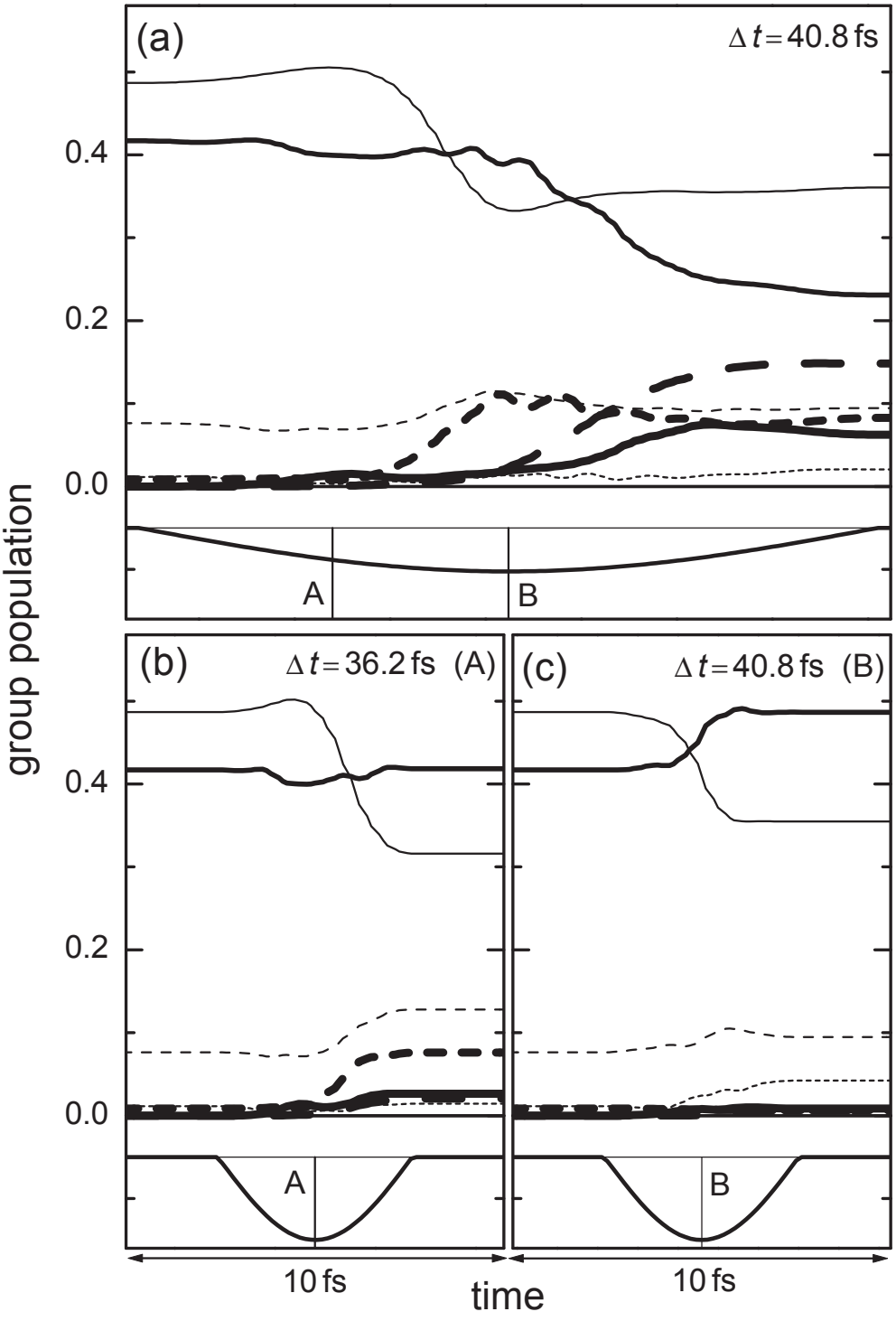
(a)
Δt = 40.8 fs
0.4
0.2
0.0
A
B
(b)
Δt = 36.2 fs (A)
(c)
Δt = 40.8 fs (B)
group population
10 fs
10 fs
time

FIG. 11:

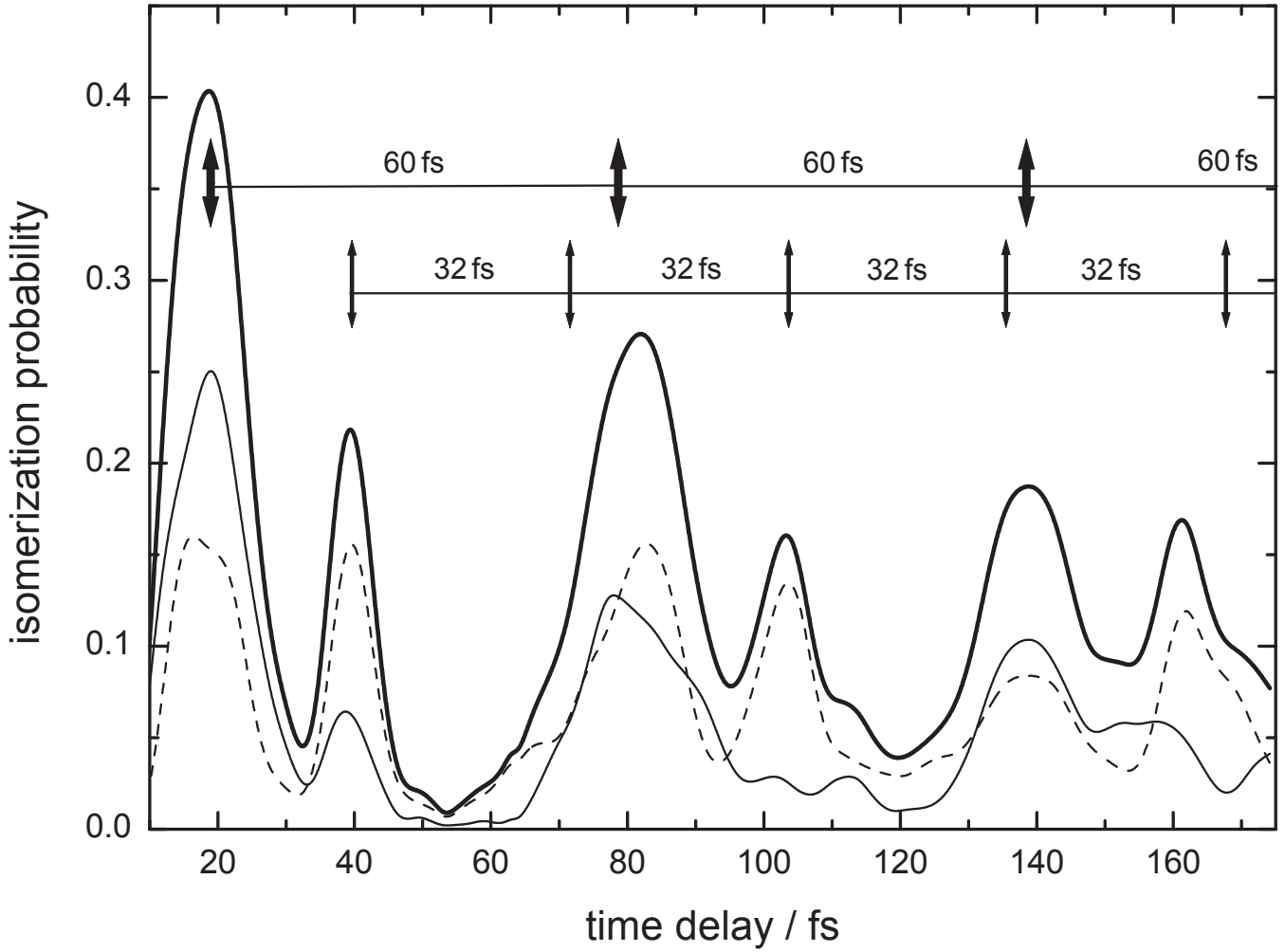
isomerization probability
time delay / fs
0.0
0.1
0.2
0.3
0.4
20
40
60
80
100
120
140
160
60 fs
60 fs
60 fs
32 fs
32 fs
32 fs
32 fs

FIG. 12: